Available online at www.sciencedirect.com
SCIENCE DIRECT
Bioorganic & Medicinal Chemistry 14 (2006) 5451–5458
Bioorganic & Medicinal Chemistry

Molecular modeling of non-covalent binding of homochiral (3*S*,3′*S*)-astaxanthin to matrix metalloproteinase-13 (MMP-13)

Zsolt Bikádi,[a] Eszter Hazai,[a] Ferenc Zsila[b] and Samuel F. Lockwood[c,*]

[a]*Virtua Drug, Ltd, H-1015 Budapest, Csalogány st. 4, Hungary*
[b]*H-2092 Budakeszi, Rózsa st. 18, Hungary*
[c]*Hawaii Biotech, Inc., 99-193 Aiea Heights Drive, Suite 200, Aiea, HI 96701, USA*

Received 5 April 2006; accepted 28 April 2006
Available online 23 May 2006

Abstract—Inhibitors for matrix metalloproteinases (MMPs) are under investigation for the treatment of various important chronic illnesses, including cancer, arthritis, and cardiovascular disease (CVD). In particular, MMP-13 is currently being probed as a potential key target in CVD and malignant disease due to its documented effects on extracellular matrix (ECM) remodeling, important in the pathophysiology of these diseases. Within the family of related mammalian MMP enzymes, MMP-13 possesses a large hydrophobic binding pocket relative to that of other MMPs. Homochiral astaxanthin (3*S*,3′*S*-AST; 3*S*,3′*S*-dihydroxy-β,β-carotene-4,4′-dione), an important antioxidant and anti-inflammatory xanthophyll carotenoid, is an active metabolite of several novel soft drugs in clinical development; it is also extensively used and tested as a human nutraceutical. In the current study, the prediction of the geometry and energetics of its binding to human MMP-13 was conducted with molecular modeling. The method used was found to predict the energy of binding of known ligands of MMP-13 with great precision. Blind docking using the whole protein target was then used in order to identify the possible binding site(s) of AST. AST was predicted to bind at several sites in close proximity to the active center. Subsequent analyses focused on the binding site at the atomic (i.e., amino acid sequence) level suggested that AST can bind to MMP-13 with high affinity and favorable energetics. Therefore, the modeling study predicts potential direct enzyme-inhibitory activity of AST against MMP-13, a behavior that may be exploited in mammalian systems in which pathological upregulation of MMP activity is paramount.

1. Introduction

The matrix metalloproteinases (MMPs) are a family of secreted and transmembrane zinc-dependent (Zn-dependent) endopeptidases that degrade proteins of the extracellular matrices (ECM) and basement membrane components.[1] To date, about 30 structurally related members have been identified, sharing a substrate specificity of proteolytic activity against several components of the ECM.[2] The interaction of cells with the ECM is critical for the normal development and function of organisms. Accordingly, MMPs play a pivotal role in the control of signals elicited by matrix molecules regulating a variety of biological functions, including tissue remodeling, wound healing, and involution of organs.[1] In contrast to the physiologic importance of MMPs in normal growth and development, chronic stimulation of their activities has been implicated in the pathogenesis of a variety of diseases, including the spread of metastatic cancer cells,[3] atherosclerosis and coronary plaque instability,[4,5] rheumatoid arthritis,[6] and neuroinflammation.[7] Inhibition of MMPs in the pathological state has been shown to prevent the progression of these diseases.[2,8]

Human MMPs are generally comprised of three domains: (1) the N-terminal propeptide domain; (2) the protease or catalytic domain (~170 amino acids), which includes the zinc binding site; and (3) the C-terminal, hemopexin-like domain required for binding of the collagen substrate.[9,10] Most of the published three-dimensional (3D) structures of MMP catalytic domains include those domains complexed with peptidic, peptidomimetic, or non-peptidic inhibitors. The 3D structures of these catalytic domains consist of three α-helices, four parallel β-sheet strands, and one anti-parallel β-sheet strand. The catalytic site is connected with a long hydrophobic S1′ pocket, which extends

Keywords: 3*S*,3′*S*-Astaxanthin; Astaxanthin; Blind docking; Homochiral astaxanthin; Matrix metalloproteinase; MMP; MMP-13; Molecular modeling.
* Corresponding author. Tel.: +1 808 220 9168; fax: +1 808 792 1343; e-mail: slockwood@hibiotech.com

0968-0896/$ - see front matter © 2006 Elsevier Ltd. All rights reserved.
doi:10.1016/j.bmc.2006.04.047

through the protein and whose size varies among the MMP family members (Fig. 1).[2,11] In addition, there are shallow S2′ and S3′ pockets that are primarily solvent exposed (Fig. 1). Most known MMP inhibitors contain a chelating moiety (e.g., hydroxamate, thiol, and/or carboxylate groups) that interact with the catalytic zinc ion. However, it was recently demonstrated that for numerous non-peptidic inhibitors (e.g., sulfonamides, phosphinamides, and/or sulfones), extensive hydrophobic interactions between the lipophilic moieties (i.e., diphenylether group) of these molecules and the S1′ pocket can be largely responsible for the binding potencies of these inhibitors.[10,11] Additionally, a novel series of highly selective MMP-13 (collagenase-3) inhibitors (pyrimidine dicarboxamides) with low nanomolar affinities were recently reported which exhibit facile and extensive hydrophobic binding in the S1′ pocket, yet show no interactions with the catalytic zinc ion.[11]

Within the MMP family, MMP-13 possesses a relatively large S1′ pocket in comparison with other related proteinases.[9] MMP-13 has also been the subject of recent investigation as a potential key target in cardiovascular and malignant diseases.[12] Homochiral astaxanthin (3*S*,3′*S*-AST), a chirally pure antioxidant and anti-inflammatory xanthophyll carotenoid,[13,14] was selected in the current study for prediction of the geometry and energetics of its potential binding to human MMP-13 using AutoDock and GROMACS molecular modeling packages. Astaxanthin (Fig. 2) is the primary active metabolite of a number of soft drugs (i.e., active in the derivatized state)[15] under development for the treatment of ischemia–reperfusion (I/R) injury,[16–18] cardiovascular inflammation,[19] and cancer chemoprevention and chemotherapy.[20–22] Astaxanthin is abundant as a dietary component of many foodstuffs (shrimp, lobsters, salmon, and crabs)[23] as well as a human nutraceutical.[24,25] The hydrophobic, small-molecule carotenoids (AST molecular weight = 596 Da) have been well characterized as chain-breaking antioxidants and physical quenchers of singlet oxygen.[26–29] They have also been implicated in gene regulation/transcription, operating through a non-retinoic acid nuclear receptor;[30–33] the molecular basis of their gene regulatory function not completely understood at present. The direct enzyme modulatory activity of these compounds is a recently recognized phenomenon.[14]

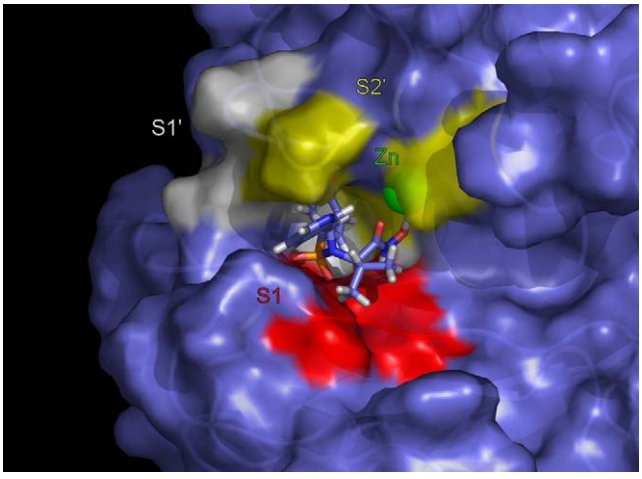

Figure 1. Solvent-accessible surface of MMP-13 complexed with a sulfonamide hydroxamic acid inhibitor (PDB code: 1EUB). The ligand binding site can be divided into several pockets (S1, S1′, and S2′). The S1′ binding pocket is relatively large compared to other members of the MMP family.

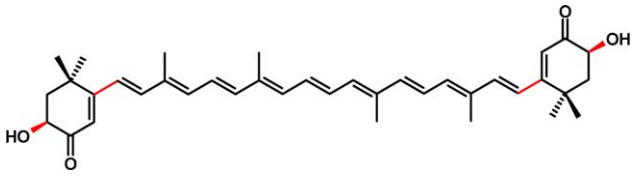

Figure 2. Chemical structure of (3*S*,3′*S*)-astaxanthin (3*S*,3′*S*-dihydroxy-β,β-carotene-4,4′-dione). Rotatable bonds are shown in red. 3*S*,3′*S*-Astaxanthin is the predominant stereoisomer in the microalgae *Haematococcus pluvialis* (>99%) utilized in nutraceutical preparations, as well as the preferred homochiral scaffold for Cardax™ soft drugs in clinical development.

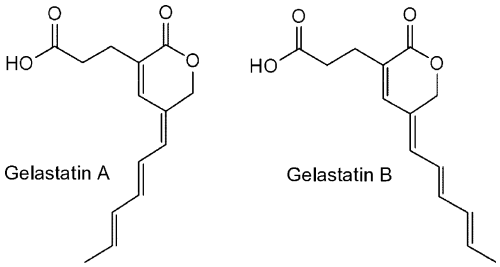

Figure 3. Chemical structures of gelastatins A and B, known inhibitors of MMP-13 (see text).

In the current study, binding of homochiral 3*S*,3′*S*-astaxanthin to MMP-13 was modeled. AST was found to bind with high affinity at or near the active site of the enzyme as documented previously for other peptidic, peptidomimetic, and lipophilic inhibitors. A common shared motif (i.e., the presence of a polyene chain) for this lipophilic small-molecule inhibitor of MMP-13 was found in the literature in an unrelated set of natural compounds (gelastatins A and B; Fig. 3). These molecules were found to exhibit MMP-inhibitory activities at the sub-micromolar (sub-μM) level.[34] This documented activity may find clinical utility in those applications requiring delivery of direct enzyme inhibitors at therapeutic concentrations.

2. Results and discussion

The available experimental human MMP-13 structures and co-crystallized ligands are summarized in Table 1. Nine human MMP-13 structures were found (3 NMR, 6 X-ray). According to the sequence alignment all sequences were fully (100.0%) identical.

As can be seen from Table 1, the backbone rmsd values of the proteins depend on the complexed ligands. Docking calculations were performed on rigid protein targets.

Table 1. Experimentally-determined structures of human MMP-13 complexed with different ligands

PDB	Procheck		Type of experiment	Res Å	Chemical names of complexed ligands	Abbr	Date of publication	rmsd (Å)
	Region	(%)						
1FLS	mf	91.7	NMR	—	*N*-Hydroxy-2-[(4-methoxy-benzenesulfonyl)-pyridin-3-ylmethyl-amino]-3-methyl-benzamide	WAY	2000	—
	aa	7.6						
	ga	0.0						
	da	0.8						
1FM1	mf	92.4	NMR	—	*N*-Hydroxy-2-[(4-methoxy-benzenesulfonyl)-pyridin-3-ylmethyl-amino]-3-methyl-benzamide	WAY	2000	0.51
	aa	6.1						
	ga	1.5						
	da	0.0						
1EUB	mf	59.3	NMR	—	1-Methyloxy-4-sulfone-benzene	MSB	2000	1.84
	aa	35.7			Hydoxyaminovaline	HAV		
	ga	5.7			3-Methylpyridine	3MP		
	da	0.0						
1XUC	mf	88.4	X-ray	1.7	*N*,*N*′-Bis(3-methylbenzyl)pyrimidine-4,6-dicarboxamide	PB3	2005	1.22
	aa	9.4						
	ga	1.1						
	da	1.1						
1XUD	mf	88.8	X-ray	1.8	*N*,*N*′-Bis(4-fluoro-3-methylbenzyl)pyrimidine-4,6-dicarboxamide	PB4	2005	1.25
	aa	9.1						
	ga	1.1						
	da	1.1						
1XUR	mf	88.4	X-ray	1.85	*N*,*N*′-Bis(pyridin-3-ylmethyl)pyrimidine-4,6-dicarboxamide	PB5	2005	1.21
	aa	9.4						
	ga	1.8						
	da	0.4						
1YOU	mf	84.0	X-ray	2.3	5-(2-Ethoxyethyl)-5-[4-(4-fluorophenoxy) phenoxy]pyrimidine-2,4,6(1*H*,3*H*,5*H*)-trione	PFD	2005	1.20
	aa	12.7						
	ga	2.2						
	da	1.1						
456C	mf	85.9	X-ray	2.4	4-[4-(4-Chloro-phenoxy)-benzenesulfonyl]-4-methyl-tetrahydro-pyran;compound with *N*-hydroxy-acetamide	345	1999	1.33
	aa	12.5						
	ga	1.1						
	da	0.4						
830C	mf	89.6	X-ray	1.6	4-[4-(4-Chloro-phenoxy)-benzenesulfonylmethyl]-tetrahydro-pyran-4-carboxylic acid hydroxyamide	RS1	1999	1.22
	aa	8.9						
	ga	1.1						
	da	0.4						

The Ramachandran analysis was performed using the Procheck program (mf: mostly favored; aa: additional allowed; ga: generously allowed; da: disallowed region). rmsd values of backbone atoms were calculated using the SWISS-PDB program[53] applying 1FLS structure as a template.

However, in living systems proteins can adopt different conformations, and such binding also depends on the nature of the bound ligand. Therefore, different experimental MMP-13 structures were considered as rigid docking targets representing different protein conformations. All of the available conformations were investigated in order to determine if (1) AST bound to MMP-13; (2) if AST bound to MMP-13, which conformation of MMP-13 was most favorable for such binding. Six human MMP-13 structures were selected for further calculations (Fig. 4).

Molecular docking is one of the most widely used techniques for calculation of protein–ligand and protein–protein interactions. De facto, molecular docking is analogous to X-ray crystallography (XRC), considering that both methods are able to create atomic representations of molecular complexes. Although automation of XRC is currently in the frontline of research, reduction of the time necessary for the obligatory preceding protein expression and purification is difficult. Moreover, measurement of macromolecular assemblies is often problematic. Given these problems, development of alternative techniques like molecular docking is of world-wide interest. 'Blind docking' was introduced for the detection of possible ligand binding sites on the whole protein target.[35,36] The 'blind docking' methodology has been proven to be a successful tool for a priori prediction of protein–ligand interactions. Docking calculations have three main functions: (1) finding potential binding site(s); (2) determining the correct binding conformation; and (3) determining the free energy of binding at a given position. Comparison of the calculated and experimental free energies of binding yields

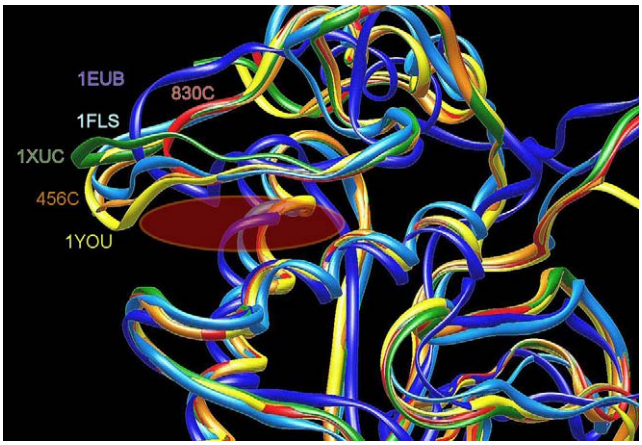

Figure 4. Selected MMP-13 structures utilized for blind docking calculations. The backbone structure around the ligand binding region (indicated with a red ellipse) is quite flexible.

an approximation of how reliable a blind docking calculation might be. In the current study, the calculations performed on different inhibitor—MMP-13 complexes gave an acceptable estimation of PFD and WAY, and excellently reproduced the experimental data for PB3, 345, and RS1 binding to MMP-13 (Table 2). The best approximation was achieved for PB3, which is a non-zinc binding inhibitor. Thus, experimental binding energies can be reproduced with great precision using the current modeling methods.

Docking calculations were carried out on all selected proteins (Fig. 4) in order to determine if AST bound to MMP-13, and if so, to which protein conformation. Three types of binding sites for astaxanthin on MMP-13 were found: (1) AST can fill up a groove near the active site of MMP-13; (2) AST can fit into a hole of the protein near the active center binding site; and (3) AST can form interactions at the surface (Figs. 5a, b, and c, respectively). The 'groove' model (Fig. 5a; derived from the calculation of the AST—1EUB complex) was calculated to possess the lowest docked energy (Table 3).

Blind docking calculations were useful for locating the binding site of AST on the target protein. Given the binding site, AST is only allowed to dock to the previously determined position. The binding mode (rotation, conformation) can be determined by focused docking, where the binding site determined with blind docking is subject to further, more detailed calculations. Protein

Table 2. Comparison of the experimental and calculated free energies of binding of various MMP-13 ligands (from literature-reported values; see Table 1)

PDB	Ligand	Experimental free energy of binding kcal/mol	Calculated free energy of binding kcal/mol
1XUC	PB3	−9.7	−9.4
1YOU	PFD	−12.3	−8.5
1FLS	WAY	−10.2	−7.7
456C	345	−13.3	−12.5
830C	RS1	−12.6	−11.7

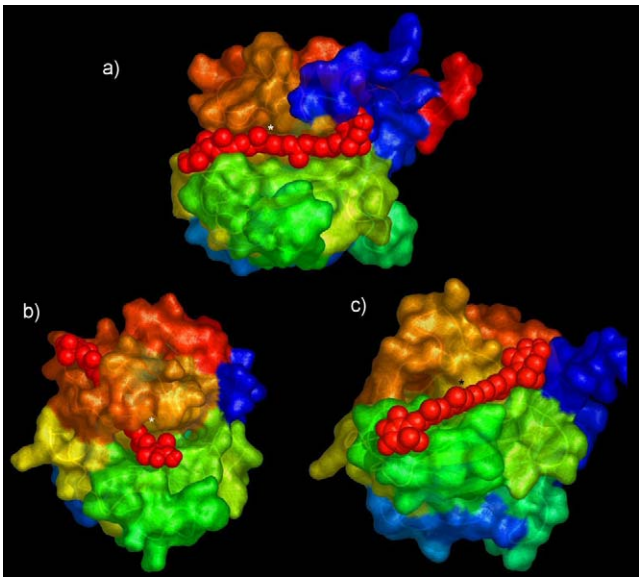

Figure 5. The best-ranked blind docking results for AST–MMP-13 binding. (a) AST (red) fits into the groove at the active center (groove-PDB code: 1EUB); (b) AST spans a hole near the active center binding site (hole-PDB code: 1FLS); (c) AST forms interactions at the surface (surf-PDB code: 1YOU). The star symbol (*) indicates the catalytic zinc (Zn) position.

Table 3. Calculated 'docked' energies (see text) of the best-ranked results of blind docking calculations on different protein models (see also Fig. 5)

Rank	Docked energy (kcal/mol)	Hit	Type	Protein model
1	−14.93	8	Groove	1EUB
2	−12.27	4	Hole	1FLS
3	−11.78	1	Hole	456C
4	−11.27	7	Hole	1XUC
5	−11.10	4	Surf	1YOU
6	−11.08	2	Groove	830C

sidechain flexibility is gained by molecular dynamics (MD) calculations. Focused docking calculations revealed that the conformation of MMP-13 represented by 1EUB bound astaxanthin with the lowest intermolecular energy. The intermolecular energy was calculated to decrease during the first 0.1 ps of the MD simulation, but was higher at 1 ps (−12.53 kcal/mol). The calculated intermolecular energy at 0.1 ps was −15.15 kcal/mol, the lowest value among the investigated ligands. Analysis of interacting protein sidechains revealed that AST was bound in the groove mostly by hydrophobic interactions (Fig. 6).

The terminal β-ionone rings of AST exhibited both hydrophobic and hydrophilic interactions with MMP-13 (Fig. 6). Specifically, one ring formed a hydrogen (H–) bond with T110 and also formed a hydrophobic interaction with L111. The other ring made an intermolecular H-bond with the phenolic –OH group of Y214 and was in π–π interaction with Y244. The polyene chain fitted in the apolar groove established numerous hydrophobic and π–π stacking interactions with amino acid residues, as indicated in Figure 6 and Table 4.

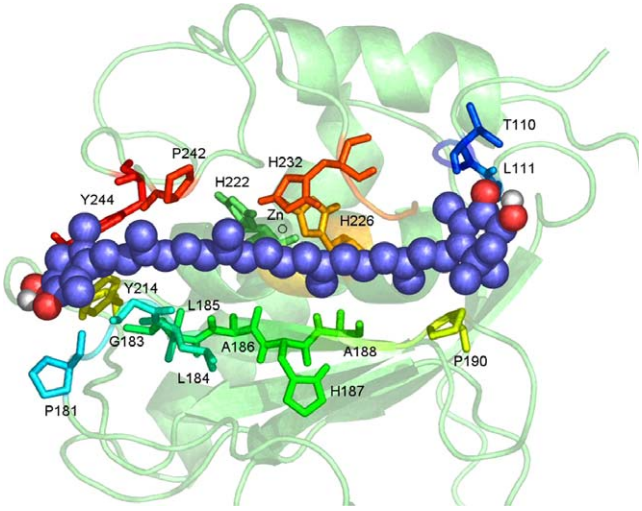

Figure 6. Amino acid residues within 4 Å distance of 3*S*,3′*S*-AST (in space-filling representation) at the 'groove' binding site of MMP-13, as revealed by the docking calculations using the 1EUB X-ray structure. The AST ligand molecule forms numerous hydrophobic interactions with alanine, leucine, tyrosine, proline, and histidine residues (denoted by their one-letter amino acid codes).

Binding modes 'hole' and 'surf' were calculated to possess somewhat higher docking energies than 'groove' (Figs. 5b and c and Table 3). However, these energies were comparable to those reported for experimentally determined bound ligands (cf. Table 2); therefore, the 'hole' and 'surf' binding modes could also play a role in the interaction of AST with MMP-13.

The antioxidant behaviors of carotenoids, including both 'carotenes' (completely hydrocarbon compounds) and 'xanthophylls' (oxygen-substituted molecules), are well established in the literature.[37] Most of these studies have been performed in organic solvent model systems and/or liposome systems. As radical chain-breakers and physical quenchers of singlet oxygen, they share this dual antioxidant capability with vitamins E and C.[38] Recently, the ability of both pro-vitamin A ('retinoids'; e.g., β-carotene) and non-pro-vitamin A carotenoids (including astaxanthin) to act as gene-regulatory agents has emerged.[30,32,33] As anti-inflammatory agents, the emerging literature suggests that this function may possibly be secondary to the antioxidant role, that is, regulation of systemic redox status may downregulate central inflammation pathways such as NF-κB.[39–41] A role as direct enzyme inhibitors has only recently been suggested.[14]

In a mouse peritoneal inflammation model, Lockwood et al. demonstrated a generalized in vivo antioxidant capability for oral Cardax™, an astaxanthin-based soft drug which releases AST after both oral and parenteral administration.[13] This was exhibited as a reduction in 8-isoprostane-$F2_\alpha$ at the time point of maximal neutrophilic recruitment and activation in that model, thus confirming in vivo antioxidant capability as demonstrated in a pilot oral I/R rodent study.[18] However, at the time points of maximal monocyte/macrophage recruitment and activation, two molecular fingerprints of the activity of 5-lipoxygenase (5-LO)[42] were significantly reduced, namely 5-HETE and 5-oxo-EET. Working backwards from the in vivo molecular fingerprint data, the authors subsequently confirmed direct in vitro interaction of the optically inactive *meso*-Cardax™ compound with human 5-LO with circular dichroism (CD) spectroscopy.[14] Molecular modeling of this potential interaction (using rabbit 15-LO as a surrogate, as XRC data for mammalian 5-LO have not been reported) demonstrated interactions between *meso*-Cardax™ and the solvent-exposed surface of the enzyme. Hence, direct interaction (i.e., inhibition) of mammalian enzymes by carotenoids may be possible and not indirectly through antioxidant activity (i.e., modulation of redox status).

The results of the current study extend these prior results. 3*S*,3′*S*-AST appears capable of high-affinity binding to MMP-13, an important enzyme in the ECM remodeling which takes place in both CVD[43–46] and

Table 4. Protein residues of MMP-13 involved in binding interactions with AST

Residues interacting with astaxanthin	Experimentally determined interactions with MMP-13 inhibitors						Type of interaction
1EUB	1XUC	830C	456C	1YOU	1FLS	1EUB	
T110							Hydrophilic
L111							Hydrophobic
P181							Hydrophobic
G183		RS1			WAY	3MP	Hydrophobic
L184		RS1			WAY	HAV	Hydrophobic
L185		RS1	345	PFD	WAY	MSB	Hydrophobic
A186		RS1	345	PFD		HAV	Hydrophobic
H187							Hydrophobic
A188		RS1	345				Hydrophobic
P190							Hydrophobic
Y214							Hydrophilic
H222	PB3	RS1	345	PFD	WAY	MSB	Hydrophobic
H226		RS1	345		WAY		Hydrophobic
H232		RS1		PFD	WAY		Hydrophobic
P242		RS1	345			3MP	Hydrophobic
Y244	PB3	RS1	345	PFD	WAY	MSB	Hydrophobic

The same amino acids involved in binding of known inhibitors are also indicated.

cancer. To the authors' knowledge, this is the second such suggestion of potential direct enzyme inhibition for a xanthophyll carotenoid.[14] In a rabbit atherosclerosis model, a Scandinavian group found favorable effects of oral AST on markers of plaque vulnerability and inflammation, including macrophage recruitment and protein levels of MMP-3.[47,48] Whether the reduction in MMP-3 protein levels was secondary to non-significant antioxidant activity on ex vivo LDL-oxidation capability by AST was not investigated in that study. We suggest that the current results are compatible with a recently recognized ability of xanthophyll carotenoids such as AST to directly interact with mammalian enzymes important in chronic diseases such as CVD.

3. Conclusion

In summary, docking calculations were performed in order to predict the potential binding ability of homochiral 3*S*,3′*S*-astaxanthin to MMP-13. It was concluded that astaxanthin was likely to bind to MMP-13 with an affinity comparable with known X-ray ligands, at sites at or near the active center of the enzyme. Because the calculated binding sites were at or near to the catalytic site, the current results suggest that AST has potential inhibitory activity on MMP-13, and as such, may find clinical utility in those indications where modulation of metalloproteinase activity is therapeutically relevant.

4. Experimental

Experimental MMP-13 structures were derived from the Protein Data Bank [1EUB,[49] 1FLS,[50] 1FM1,[50] 1XUC,[11] 1XUD,[11] 1YOU,[51] 1XUR,[11] 456C,[9] and 830C[9]]. The quality of the models was analyzed by the Procheck program.[52] Monomeric proteins were extracted from PDB files, and 'A' chains were used for further studies in each case. Water and ligand molecules were removed from the structures. The Swiss-PDB program[53] was applied for structural alignment of the available MMP-13 structures using the 1FLS entry as a template. The structures were divided into groups based on their backbone structures. In each group, the structure with the best quality result from the Procheck analysis was selected for further calculations.

MMFF94 force field[54] was used for energy minimization of (3*S*,3′*S*)-astaxanthin (Fig. 2). The conjugate gradient method was applied during the calculations. Gasteiger partial charges were added to the ligand atoms. Non-polar hydrogen atoms were merged, and rotatable bonds were defined with the aid of Autodock tools (Fig. 2).[55]

A selected set of six human MMP-13 was used for the docking calculations. Essential hydrogen atoms of crystal structures, Kollman united atom type charges, and solvation parameters were added with the aid of AutoDock tools.[55] Zinc ion radius $r = 1.48$ Å and well depth $\varepsilon = 0.550$ kcal/mol were used for generation of grid and docking parameter files. Affinity (grid) maps of 200 grid points in each Cartesian direction and 0.375 Å spacing were generated using the Autogrid program.[55] Maps were centered on the protein center (PHE224). AutoDock parameter set- and distance-dependent dielectric functions were used in the calculation of the van der Waals and the electrostatic terms, respectively. Docking simulations were performed using the Lamarckian genetic algorithm (LGA) and the Solis & Wets local search method[56] of Autodock.[55] Initial position, orientation, and torsions of the ligand molecule were set randomly. All rotatable torsions of AST (Fig. 2) were released during docking. Each docking experiment was derived from 100 different runs that were set to terminate after a maximum of 1,500,000 energy evaluations. The population size was set to 250. During the search, a translational step of 0.2 Å, and quaternion and torsion steps of 5 were applied. Binding free energies of each job were collected and the minima were selected. Root mean squared deviation (rmsd) was calculated for the resulting 100 structures using ligand structures of minimum energies at each job as references. A 2.0 Å tolerance was used to form clusters of the closest structures.

The complex structure corresponding to the lowest calculated free energy of binding was used for structure refinement. Smaller grid maps, namely 100 grid points in each Cartesian direction, and 0.375 Å spacing (centered on the ligand center of the result of blind docking calculations), were generated using the Autogrid program. The same procedure was applied for focused docking calculations as was described for the blind docking calculations, except that the number of runs was set to 10 and the population size was 50.

Molecular dynamics calculations were carried out on the lowest energy complex. The GROMACS program package[57] was applied for generation of a simulation box and addition of explicit water molecules and counter ions. Complexes were energy-minimized using the GROMOS force field[58] implemented in the program package. Short 0.1 picosecond (ps) and 1 ps long unrestrained molecular dynamics simulations (MD), which improved greatly the prediction of binding affinities in calculation of HIV-1-protease inhibitor complexes,[59] were performed to equilibrate the surrounding molecules and to generate conformations for calculations of intermolecular interaction energy using Autodock.

To calculate the binding energies of experimentally available MMP-13–inhibitor complexes with AutoDock, ligand coordinates were extracted from the corresponding PDB files. AutoDock tools were used for adding hydrogen atoms to the ligands and for calculating Gasteiger partial charges on the atoms. Non-polar hydrogens were merged. Affinity (grid) maps of 100 grid points in each Cartesian direction and 0.375 Å spacing were generated with the aid of Autogrid. Maps were centered on the original position of ligand molecules. Free energy of binding values were calculated using the command mode of AutoDock. The experimental binding energies were converted from the experimental inhibition constants (K_i), using the equation: $\Delta G_0 = -RT \ln K_i$ where ΔG_0 is the Gibbs' free energy of binding (kcal/mol), R is the gas constant

(1.987 cal K^{-1} mol^{-1}), and T is the absolute temperature (room temperature, 300 K). The binding energies of MMP-13–AST complexes after MD calculation were obtained similarly. Input complex coordinates were prepared by separating 0.1 ps and 1 ps snapshots recorded from MD simulations into one file containing only MMP-13 structure, and one file containing only the ligand coordinates. The free energy of binding of AST to MMP-13 was calculated after 0.1 ps and after 1 ps with the command mode of AutoDock.

Acknowledgment

The authors wish to thank Dave M. Watumull for helpful formatting and bibliographic assistance during the preparation of the manuscript.

References and notes

1. Sternlicht, M. D.; Werb, Z. *Annu. Rev. Cell Dev. Biol.* **2001**, *17*, 463.
2. Skiles, J. W.; Gonnella, N. C.; Jeng, A. Y. *Curr. Med. Chem.* **2004**, *11*, 2911.
3. Demers, M.; Couillard, J.; Belanger, S.; St-Pierre, Y. *Crit. Rev. Immunol.* **2005**, *25*, 493.
4. Galis, Z. S.; Khatri, J. J. *Circ. Res.* **2002**, *90*, 251.
5. Tayebjee, M. H.; Lip, G. Y.; MacFadyen, R. J. *Curr. Med. Chem.* **2005**, *12*, 917.
6. Burrage, P. S.; Mix, K. S.; Brinckerhoff, C. E. *Front. Biosci.* **2006**, *11*, 529.
7. Yong, V. W. *Nat. Rev. Neurosci.* **2005**, *6*, 931.
8. Bachmeier, B. E.; Iancu, C. M.; Jochum, M.; Nerlich, A. G. *Expert Rev. Anticancer Ther.* **2005**, *5*, 149.
9. Lovejoy, B.; Welch, A. R.; Carr, S.; Luong, C.; Broka, C.; Hendricks, R. T.; Campbell, J. A.; Walker, K. A.; Martin, R.; Van Wart, H.; Browner, M. F. *Nat. Struct. Biol.* **1999**, *6*, 217.
10. Skiles, J. W.; Gonnella, N. C.; Jeng, A. Y. *Curr. Med. Chem.* **2001**, *8*, 425.
11. Engel, C. K.; Pirard, B.; Schimanski, S.; Kirsch, R.; Habermann, J.; Klingler, O.; Schlotte, V.; Weithmann, K. U.; Wendt, K. U. *Chem. Biol.* **2005**, *12*, 181.
12. Leeman, M. F.; Curran, S.; Murray, G. I. *Crit. Rev. Biochem. Mol. Biol.* **2002**, *37*, 149.
13. Lockwood, S. F.; Gross, G. J. *Cardiovasc. Drug Rev.* **2005**, *23*, 199.
14. Lockwood, S. F.; Penn, M. S.; Hazen, S. L.; Bikádi, Z.; Zsila, F. *Life Sci.*, **2006,** in press.
15. Bodor, N. *Pharmazie* **2001**, *56*, S67.
16. Gross, G. J.; Lockwood, S. F. *Life Sci.* **2004**, *75*, 215.
17. Gross, G. J.; Lockwood, S. F. *Mol. Cell. Biochem.* **2005**, *272*, 221.
18. Gross, G. J.; Hazen, S. L.; Lockwood, S. F. *Mol. Cell. Biochem.* **2006**, *283*, 23.
19. Lauver, D. A.; Lockwood, S. F.; Lucchesi, B. R. *J. Pharmacol. Exp. Ther.* **2005**, *314*, 686.
20. Hix, L. M.; Lockwood, S. F.; Bertram, J. S. *Cancer Lett.* **2004**, *211*, 25.
21. Hix, L. M.; Frey, D. A.; McLaws, M. D.; Østerlie, M.; Lockwood, S. F.; Bertram, J. S. *Carcinogenesis* **2005**, *26*, 1634.
22. King, T. J.; Bertram, J. S. *Biochim. Biophys. Acta* **2005**, *1719*, 146.
23. Turujman, S. A.; Wamer, W. G.; Wei, R. R.; Albert, R. H. *J. AOAC Int.* **1997**, *80*, 622.
24. Spiller, G. A.; Dewell, A. *J. Med. Food* **2003**, *6*, 51.
25. Higuera-Ciapara, I.; Felix-Valenzuela, L.; Goycoolea, F. M. *Crit. Rev. Food Sci. Nutr.* **2006**, *46*, 185.
26. Miki, W. *Pure Appl. Chem.* **1991**, *63*, 141.
27. Shimidzu, N.; Goto, M.; Miki, W. *Fisheries Sci.* **1996**, *62*, 134.
28. Cardounel, A. J.; Dumitrescu, C.; Zweier, J. L.; Lockwood, S. F. *Biochem. Biophys. Res. Commun.* **2003**, *307*, 704.
29. Chew, B. P.; Park, J. S. *J. Nutr.* **2004**, *134*, 257S.
30. Bertram, J. S. *Nutr. Rev.* **1999**, *57*, 182.
31. Bertram, J. S.; Vine, A. L. *Biochim. Biophys. Acta* **2005**, *1740*, 170.
32. Hix, L. M.; Lockwood, S. F.; Bertram, J. S. *Redox Rep.* **2004**, *9*, 181.
33. Hix, L. M.; Vine, A. L.; Lockwood, S. F.; Bertram, J. S. In *Carotenoids and Retinoids: Molecular Aspects and Health Issues*; Packer, L., Obermueller-Jevic, U., Kraemer, K., Sies, H., Eds.; AOCS: Champaign, IL, 2005; pp 182–203.
34. Lee, H. J.; Chung, M. C.; Lee, C. H.; Chun, H. K.; Rhee, J. S.; Kho, Y. H. *Ann. N.Y. Acad. Sci.* **1999**, *878*, 635.
35. Hetényi, C.; van der Spoel, D. *Protein Sci.* **2002**, *11*, 1729.
36. Hetényi, C.; van der Spoel, D. *FEBS Lett.* **2006**, *580*, 1447.
37. Britton, G. *FASEB J.* **1995**, *9*, 1551.
38. Papas, A. M. *Mature Med.* **1999**, *Nov./Dec.*, 315.
39. Lee, S. J.; Bai, S. K.; Lee, K. S.; Namkoong, S.; Na, H. J.; Ha, K. S.; Han, J. A.; Yim, S. V.; Chang, K.; Kwon, Y. G.; Lee, S. K.; Kim, Y. M. *Mol. Cells* **2003**, *16*, 97.
40. Ohgami, K.; Shiratori, K.; Kotake, S.; Nishida, T.; Mizuki, N.; Yazawa, K.; Ohno, S. *Invest. Ophthalmol. Vis. Sci.* **2003**, *44*, 2694.
41. Suzuki, Y.; Ohgami, K.; Shiratori, K.; Jin, X. H.; Ilieva, I.; Koyama, Y.; Yazawa, K.; Yoshida, K.; Kase, S.; Ohno, S. *Exp. Eye Res.* **2006**, *82*, 275.
42. Zhang, R.; Brennan, M. L.; Shen, Z.; MacPherson, J. C.; Schmitt, D.; Molenda, C. E.; Hazen, S. L. *J. Biol. Chem.* **2002**, *277*, 46116.
43. Lee, W. H.; Kim, S. H.; Lee, Y.; Lee, B. B.; Kwon, B.; Song, H.; Kwon, B. S.; Park, J. E. *Arterioscler. Thromb. Vasc. Biol.* **2001**, *21*, 2004.
44. Yoon, S.; Kuivaniemi, H.; Gatalica, Z.; Olson, J. M.; Buttice, G.; Ye, S.; Norris, B. A.; Malcom, G. T.; Strong, J. P.; Tromp, G. *Matrix Biol.* **2002**, *21*, 487.
45. Deguchi, J. O.; Aikawa, E.; Libby, P.; Vachon, J. R.; Inada, M.; Krane, S. M.; Whittaker, P.; Aikawa, M. *Circulation* **2005**, *112*, 2708.
46. Gough, P. J.; Gomez, I. G.; Wille, P. T.; Raines, E. W. *J. Clin. Invest.* **2006**, *116*, 59.
47. Li, W.; Hellsten, A.; Jacobsson, L. S.; Blomqvist, H. M.; Olsson, A. G.; Yuan, X. M. *J. Mol. Cell. Cardiol.* **2004**, *37*, 969.
48. Jacobsson, L. S.; Yuan, X. M.; Zieden, B.; Olsson, A. G. *Atherosclerosis* **2004**, *173*, 231.
49. Zhang, X.; Gonnella, N. C.; Koehn, J.; Pathak, N.; Ganu, V.; Melton, R.; Parker, D.; Hu, S. I.; Nam, K. Y. *J. Mol. Biol.* **2000**, *301*, 513.
50. Moy, F. J.; Chanda, P. K.; Chen, J. M.; Cosmi, S.; Edris, W.; Levin, J. I.; Powers, R. *J. Mol. Biol.* **2000**, *302*, 671.
51. Blagg, J. A.; Noe, M. C.; Wolf-Gouveia, L. A.; Reiter, L. A.; Laird, E. R.; Chang, S. P.; Danley, D. E.; Downs, J. T.; Elliott, N. C.; Eskra, J. D.; Griffiths, R. J.; Hardink, J. R.; Haugeto, A. I.; Jones, C. S.; Liras, J. L.; Lopresti-Morrow, L. L.; Mitchell, P. G.; Pandit, J.; Robinson, R. P.; Subramanyam, C.; Vaughn-Bowser, M. L.; Yocum, S. A. *Bioorg. Med. Chem. Lett.* **2005**, *15*, 1807.
52. Laskowski, R. A.; MacArthur, M. W.; Moss, D. S.; Thornton, J. M. *J. Appl. Crystallogr.* **1993**, *26*, 283.

53. Guex, N.; Peitsch, M. C. *Electrophoresis* **1997**, *18*, 2714.
54. Halgren, T. A. *J. Am. Chem. Soc.* **1992**, *114*, 7827.
55. Morris, G. M.; Goodsell, D. S.; Halliday, R. S.; Huey, R.; Hart, W. E.; Belew, R. K.; Olson, A. J. *J. Comput. Chem.* **1998**, *19*, 1639.
56. Solis, F. J.; Wets, R. J.-B. *Math. Oper. Res.* **1981**, *6*, 19.
57. Berendsen, H. J. C.; van der Spoel, D.; van Drunen, R. *Comput. Phys. Commun.* **1995**, *91*, 43.
58. Hermans, J.; Berendsen, H. J. C.; Van Gunsteren, W. F.; Postma, J. P. M. *Biopolymers* **1984**, *23*, 1513.
59. Jenwitheesuk, E.; Samudrala, R. *BMC Struct. Biol.* **2003**, *3*, 2.